In vivo degradation and endothelialization of an iron bioresorbable scaffold

Wenjiao Lin[a,b], Hongjie Zhang[c], Wanqian Zhang[b,c], Haiping Qi[b], Gui Zhang[d], Jie Qian[e], Xin Li[c], Li Qin[b], Haifeng Li[b], Xiang Wang[a], Hong Qiu[e], Xiaoli Shi[b,f], Wei Zheng[a,*], Deyuan Zhang[b,**], Runlin Gao[e,***], Jiandong Ding[c,****]

[a] College of Materials Science and Chemical Engineering, Harbin Engineering University, Harbin 150001, China
[b] Biotyx Medical (Shenzhen) Co., Ltd, Shenzhen 518109, China
[c] State Key Laboratory of Molecular Engineering of Polymers, Department of Macromolecular Science, Fudan University, Shanghai 200438, China
[d] Shenzhen Advanced Medical Services Co., Ltd, Shenzhen, 518000, Guangdong, China
[e] Department of Cardiology, Fuwai Hospital, National Center for Cardiovascular Diseases, Chinese Academy of Medical Sciences and Peking Union Medical College, Beijing 100037, China
[f] Key Laboratory of Advanced Technology for Materials of Education Ministry, School of Materials Science and Engineering, Southwest Jiaotong University, Chengdu 610031, China

ARTICLE INFO

ABSTRACT

Detection of in vivo biodegradation is critical for development of next-generation medical devices such as bioresorbable stents or scaffolds (BRSs). In particular, it is urgent to establish a nondestructive approach to examine in vivo degradation of a new-generation coronary stent for interventional treatment based on mammal experiments; otherwise it is not available to semi-quantitatively monitor biodegradation in any clinical trial. Herein, we put forward a semi-quantitative approach to measure degradation of a sirolimus-eluting iron bioresorbable scaffold (IBS) based on optical coherence tomography (OCT) images; this approach was confirmed to be consistent with the present weight-loss measurements, which is, however, a destructive approach. The IBS was fabricated by a metal-polymer composite technique with a polylactide coating on an iron stent. The efficacy as a coronary stent of this new bioresorbable scaffold was compared with that of a permanent metal stent with the name of trade mark Xience, which has been widely used in clinic. The endothelial coverage on IBS was found to be greater than on Xience after implantation in a rabbit model; and our well-designed ultrathin stent exhibited less individual variation. We further examined degradation of the IBSs in both minipig coronary artery and rabbit abdominal aorta models. The present result indicated much faster iron degradation of IBS in the rabbit model than in the porcine model. The semi-quantitative approach to detect biodegradation of IBS and the finding of the species difference might be stimulating for fundamental investigation of biodegradable implants and clinical translation of the next-generation coronary stents.

1. Introduction

As an implantable medical device with high risk, an ideal bioresorbable stents or scaffolds (BRSs) should not only demonstrate safety and effectiveness non-inferior to the current permanent drug-eluting stents [1,2], but also exhibit advantages of decreasing long-term risks, improving very late clinical outcomes [3], leaving the unrestricted vascular growth of infants or kids [4,5] and allowing the possible re-intervention [6]. The first BRS – Igaki-Tamai scaffold composed of polylatide (PLA) was implanted into human coronary artery in 1998 [7], and more than 20 years go through since then. In 2017 the thick-strut Absorb (157 μm PLA, Abbott) bioresorbable vascular scaffold was withdrawn from the market in 2017 after getting CE mark in 2011 and US Food and Drug Agency (FDA) approval in 2016. Although the road of BRS is full of twists and turns, BRS is still promising as the next-generation stent. So far, many thick-strut (ranging from 150 to 170 μm)

polymeric and metallic BRSs are available for commercial use in clinical practice. For example, two BRSs, Magmaris (164 μm magnesium, Biotronik, Germany) [8] and ART-BRS (170 μm PLA, Arterial Remodeling Technologies, France) were approved by CE, and two BRSs, Neovas (170 μm PLA, Lepu, China) [9] and Xinsorb (160 μm PLA, Huaan, China) were approved by China National Medical Products Administration [10]. While permanent thin-strut stents gradually demonstrate noninferiority or superiority to state-of-the-art permanent stents [11–14], resulting in more rapid endothelial coverage [15] and thus decreased stent thrombosis (ST) and myocardial infarction [16], an increasing number of novel designed thin-strut polymeric and metallic BRSs are emerging and coming into market or clinical trials [17], including MeRes100 (100 μm PLA, Meril Life Science, India) [18], DESolve Cx (120 μm PLA, Elixir, USA) and Fantom (125 μm polycarbonate, REVA, USA) with CE Mark in 2016–2019, IBS (73 μm iron, Biotyx, China) [19], Magnitude (98 μm PLA, Amaranth Medical, USA) and Firesorb (100–125 μm PLA, Microport, China) [20] in clinical research. The future direction of BRS iteration is of thin struts, reduced vessel wall coverage area and sufficient radial strength [21–23].

Adequate and proper experimental animals and pre-clinical follow-ups are very important for a clinical success of any BRS. However, the preclinical studies in animals so far have limitations to predict scaffold performance in human. For example, endothelialization rates are known to be faster in pigs than in rabbits [24], and be faster in non-human animal models than in humans [17]. Even with abundant studies in a variety of animal models, Absorb (cohort A to cohort B) and Magmaris (DREAMS 1G to DREAMS 2G) still suffer from setbacks in feasible clinical trials due to much faster degradation than expected [25,26], which suggests that the degradation in human coronary artery might be significantly different from that in some animal models. The primary reason is that the stented vessels with less than 30% patency are stenosed or atherosclerotic in patients, but the stented vessels are always healthy or slight diseased in animal models. Delayed vessel healing and severe deviation of the BRS degradation profile from the designed one probably ruin the safety and effectiveness of BRS. Further, the individual variation might also present huge challenge to BRS design. There are restenosis case reports in the post-market clinical use that Magmaris scaffold collapsed with premature dismantling 8 days after human coronary implantation [27], while collapsed scaffolds with nonabsorbed struts were found by optical coherence tomography (OCT) 20 months after clinical implantation [28].

Biodegradation rates and processes are important topics for regenerative biomaterials [29–33]. The degradation profile in human is critical for evaluating risks and the follow-up time in clinical trials. Both Absorb and Magmaris obtained CE mark using only 1-year clinical follow-up outcomes; however, the complete degradation period of Absorb is around 3 years while that of Magmaris is around 1 year [26]. The degradation peak during 2–3 years after human coronary implantation of Absorb together with the asymmetric spatial degradation of PLA [34] caused significant higher thrombosis and target lesion revascularization when compared to the permanent drug-eluting stent Xience at 2-year and 3-year clinical follow-ups. Hence, in order to fully evaluate the degradation profile of the scaffold, the follow-up time should cover the whole degradation period [1] which varies among different BRSs. With similar materials and degradation period to Absorb, the Neovas and Xinsorb PLA BRSs were required to show 3-year clinical follow-up outcomes before approved for market. For the iron-based bioresorbable scaffold, the proper animal model for evaluation of degradation, which is closer to that in human coronary artery, should be identified. In addition, the ability to detect the time course of in vivo degradation is essential to design biomedical devices [35]. There are some methods to evaluate in vivo degradation of absorbable stents. The most common one is weight-loss measurement which is quantitative, reliable, however, destructive with lots of animals sacrificed; it is not suitable for clinical follow-up. Some other methods, such as OCT and intravascular ultrasound (IVUS), are non-destructive but not

quantitative. The qualitative evaluation iron degradation by OCT had been demonstrated by our previous work [36]. However, a semi-quantitative degradation evaluation method has not yet been reported by any group. It is urgent to establish a nondestructive but semi-quantitative way to evaluate the degradation profile of a BRS based on animal models, which is of much importance in the later clinical trials and applications.

To address these concerns, herein we tried to establish a semi-quantitative modality by OCT to evaluate the in vivo degradation of an iron based stent IBS, aiming to prepare for the follow-up of degradation of IBS in the future clinical trial. The sirolimus-eluting iron bioresorbable scaffold with the trademark name IBS was fabricated by employing a core technique called metal-polymer composite [37–39]. We also compared the endothelialization extents and endothelial function restoration between ultrathin IBS (73 μm in total, Biotyx, China) and a permanent thin-strut drug-eluting stent Xience (96 μm in total, Abbott, USA) after implanted in the rabbit iliac arteries. Last but not least, it is the first time to investigate dependence of material degradation of IBS coronary stents upon animal models and individual variation.

2. Materials and methods

2.1. Materials

We made the IBS platform using pure iron alloyed with nitrogen. The alloying may increase the degradation rate and improve the mechanical properties [40,41]. The current sirolimus-eluting iron bioresorbable scaffolds (IBS Z8-P20 scaffolds, Φ3.0 × 8 mm & Φ3.0 × 15 mm, 800 nm zinc buffer layer, total coating thickness of both luminal and abluminal sides ~20 μm), IBS Z8-P13 scaffolds (Φ3.0 × 8 mm, 800 nm zinc buffer layer, total coating thickness ~13 μm), IBS Z6-P13 scaffolds (Φ3.0 × 8 mm, 600 nm zinc buffer layer, total coating thickness ~13 μm), and 316L stainless steel P13 stents (Φ3.0 × 8 mm, total coating thickness ~13 μm) shared the same ultrathin (53 μm) IBS platform design and sirolimus density (1.4 μm/mm^2). All of these stents or scaffolds were manufactured by Biotyx Medical Co., Ltd. (Shenzhen, China). The IBS series of scaffolds were laser cut from nitrided iron tube, electrochemically polished, loaded with gold radiopaque markers, covered with a zinc buffer layer, sprayed with asymmetric sirolimus-loaded poly(D,L-lactic acid) (PDLLA, amorphous; Evonik Industries, Essen, Germany) coating resulting from inner surface shielding by a stainless steel pin placed in the central axis of the scaffold during spraying, and then crimped onto balloon of rapid exchange catheter of corresponding sizes and finally ethylene oxide sterilized. As a control, the 316L stainless steel stents also underwent laser-cutting, electrochemical polishing, coating, crimping and sterilization. A clinically widely-used polymer-coated drug-eluting Co–Cr alloy stent (Xience Prime™, Φ3.0 × 15 mm, metallic strut thickness – 81 μm and drug dose – 1.0 μg/mm^2, Abbott Vascular, Santa Clara, CA, USA) was chosen as the control for endothelialization evaluation.

2.2. Animal models and implantation

The iliac artery model of a New Zealand rabbit was chosen to evaluate the difference of endothelialization extents and endothelial cell function restoration between IBS Z8-P20 and Xience Prime. The animals received aspirin (~40 mg PO) 24 h prior to surgery, which lasted for a maximum of 45 days. The left and right iliac arteries of 6 rabbits were injured by balloon endothelial denudation. A 3.0 mm × 8 mm standard angioplasty balloon catheter was placed in the distal iliac artery over a guide wire using fluoroscopic guidance and inflated to 8 ATM with 50:50 contrast/saline. The catheter then was withdrawn proximally in its inflated state approximately to the level of the iliac bifurcation. The balloon was deflated, repositioned in the distal iliac, and vessel denudation at 10 ATM was then repeated over the same section of vessel initially denuded. Immediately following balloon

denudation, a hybrid implantation mode was adopted with every rabbit implanted with one IBS Z8-P20 ($\Phi 3.0 \times 15$ mm) in either of the denuded segment of the two iliac arteries and one Xience ($\Phi 3.0 \times 15$ mm) in the other iliac artery. The pre-mounted stent/catheter was delivered into the distal iliac artery over a guide wire using fluoroscopic guidance. IBS Z8-P20 stents were deployed at the suggested nominal inflation pressures (8 ATM) and Xience stents (10 ATM) at a target balloon to artery ratio of ~1.3 to 1.0 delivered over 30 s. Repeat angiography was performed to assess stent placement and patency. Following post-implant angiography, all catheters/sheaths were then withdrawn, all surgical wounds were closed, and all of the animals recovered.

The in vivo sirolimus release and iron degradation of IBS Z8-P20 were compared between a Bama minipig coronary artery model and a New Zealand rabbit abdominal aorta model. Forty-two IBS Z8-P20 scaffolds were implanted into 21 healthy Bama minipigs (mean weight 37 kg, range 31–43 kg) through the right femoral artery using 5F guiding catheter. Every minipig had two IBS Z8-P20 scaffolds implanted in two of the left anterior descending coronary artery (LAD), the right coronary artery (RCA) and the left circumflex artery (LCX). The stent/artery (diameter) ratio was controlled within 1.1–1.2:1. Six (n: sample number) IBS Z8-P20 scaffolded coronary vessel segments retrieved from 3 (N: animal number) minipigs were evaluated the drug release at each follow-up timepoint of 3, 7, 14, 28, 60, 90, 180 days after implantation. Another 30 IBS Z8-P20 stents were implanted in 15 minipigs, with 10 (n) retrieved IBS Z8-P20 scaffolded vessel segments from 5 (N) animals tested for in vivo iron degradation at day 28, 90 and 180 after implantation.

The New Zealand rabbit abdominal aorta model was also chosen to evaluate the difference of in vivo sirolimus release and zinc and iron degradation among IBS Z8-P20, IBS Z8-P13 and 316L stainless steel P13 stents (all were $\Phi 3.0 \times 8$ mm). The right femoral artery was surgically exposed and a 5F guide catheter was introduced over a 0.014 inches guidewire. Then, a stent was introduced and positioned in the abdominal aorta of the rabbit. Placing the stent across the orifice of major branches of the descending aorta was avoided. All rabbits (mean weight 2.5 kg, range 1.9–3.2 kg) were fed with a standard diet without cholesterol or lipid supplementation throughout the experiment.

Pooled analysis was conducted on a collection of follow-up data. For IBS Z8-P20, drug release follow-up results included data at day 7 (N = 6, n = 8), day 14 (N = 8, n = 13), day 28 (N = 8, n = 13), day 60 (N = 3, n = 5), day 90 (N = 5, n = 11) and day 180 (N = 8, n = 9) after implantation, and zinc and iron degradation follow-up results included data at day 28 (N = 8, n = 13), day 90 (N = 5, n = 11) and day 180 (N = 8, n = 9) after implantation. For IBS Z8-P13, drug release follow-up results included data at day 7 (N = 3, n = 6), day 14 (N = 4, n = 8), day 28 (N = 9, n = 11), day 60 (N = 7, n = 7), day 90 (N = 8, n = 11) and day 180 (N = 6, n = 6) after implantation, and zinc and iron degradation follow-up results included data at day 28 (N = 9, n = 11), day 90 (N = 8, n = 11) and day 180 (N = 6, n = 6) after implantation. Besides, for 316L stainless steel P13 stent, drug release follow-up results included data at day 14 (N = 5, n = 5), day 28 (N = 5, n = 5), day 54 (N = 5, n = 5), day 90 (N = 5, n = 5) and day 180 (N = 5, n = 5) after implantation.

The New Zealand rabbit abdominal aorta model was also chosen to evaluate the difference of in vivo iron degradation between IBS Z8-P13 and IBS Z6-P13 scaffolds after three months of implantation in 9 rabbits. A hybrid implantation mode was adopted with every rabbit implanted with one IBS Z8-P13 ($\Phi 3.0 \times 8$ mm) and one IBS Z6-P13 ($\Phi 3.0 \times 8$ mm) in the abdominal artery. And the implantation procedure was the same as above described.

Initial masses of the iron scaffold and zinc buffer layer were recorded for every iron-based scaffold before implantation. Use of all experimental animals in the study was in accordance with accepted institutional policies. The endothelialization study protocol was approved by the US Institutional Animal Care and Research Committee,

MedStar Research Institute Animal Facility. And the degradation study protocols using both New Zealand rabbits and Bama minipigs were approved by the Ethics Committee of the Shenzhen Advanced Medical Services Corporation in China.

2.3. Confocal microscopy and scanning electron microscopy

After 45 days of implantation in the rabbit iliac arteries, the stented iliac arteries were accessed by a ventral, midline abdominal incision and carefully dissected free from the surrounding tissues. Each explanted stent was then bisected longitudinally to expose the luminal surface and subsequently immersion fixed for 15–20 min in Zamboni's Fixative (Cat# FXZAMPT, American Master Tech Scientific Inc, Lodi, CA) at room temperature and then transferred to 15% sucrose overnight at 2 °C–8 °C before immunofluorescent staining. After incubation in 15% sucrose (pH 7.5 $\pm$ 0.1), the stented artery halves were rinsed in phosphate buffer saline (PBS). Each stent half was then subsequently stained overnight at 2 °C–8 °C for VE-Cadherin (R&D Systems Inc. NE Minneapolis, MN, dilution 1:200), a marker for endothelium with mature junctional complexes. The antibody reaction was visualized with an Alexa Fluor 555 donkey anti-goat secondary antibody (Invitrogen, Carlsbad, CA, dilution 1:150, red channel). And each stent half was also stained for P120 (Santa Cruz Biotechnology Inc, Santa Cruz, CA dilution 1:400), a marker for endothelium for junctional complexes. This antibody reaction was visualized with an Alexa Fluor 488 donkey anti-mouse secondary antibody (Invitrogen, Carlsbad, CA, dilution 1:150, green channel), while DAPI (Invitrogen, Carlsbad, CA, blue channel) was used as the nuclear counter-stain.

The extents of VE-Cadherin and P120 expression were documented at endothelial borders. Proximal segments adjacent to the stent served as a positive control for the endothelial marker. Areas showing evidence of competent barrier forming endothelial cells were defined by areas in which p120 co-localized with VE-cadherin at cell borders which showed yellow outlines resulting from mixing of red and green. Areas where only p120 localized to cell borders without evidence of VE-cadherin co-localization were scored as non-functional endothelium. Areas with neither p120 nor VE-cadherin were defined as uncovered, and correlations were made with SEM to demonstrate lack of tissue coverage. Endothelial coverage between struts was based on the area of VE-Cadherin and P120 immunostaining (mm^2) expressed as a percentage of total surface area excluding strut areas.

Following confocal microscopy observations, the above stented artery halves designated for scanning electron microscopy (SEM) were rinsed in 0.1 M sodium phosphate buffer and post-fixed in 1% osmium tetroxide for approximately 30 min. The samples were then dehydrated in a graded series of ethanol, critical-point dried, and sputter-coated with gold [42]. The specimens were visualized to estimate the extent of endothelial surface coverage above and between stent struts using SEM (S3600 N, Hitachi, Japan). The extents of strut coverage were semi-quantified by visual estimation from the proximal to distal ends. The results were expressed as a percentage of total surface area above or between struts. Endothelial cells were characteristic of spindle or polygonal shaped monolayers in close apposition.

2.4. In vivo drug release test

After vessel tissues were peeled off, the retrieved IBS scaffold was put into a brown bottle, which was then added with acetonitrile to a proper volume to make sure full immersion. Subsequently, the bottle was placed in water bath of room temperature, and treated ultrasonically for 20 min to fully extract the residual sirolimus from the scaffold. The extracts after filtration were tested for drug contents using high performance liquid chromatography (HPLC, Agilent 1260, Agilent Technologies, USA) with C18 column and a flow rate of 1 mL/min at room temperature. Sirolimus was analysed at 278 nm with acetonitrile and purified water (65:35 v/v) as the mobile phase. The released drug

for each scaffold could be calculated from the original total drug amount and the residual drug on the scaffold.

2.5. Quantitative evaluation of in vivo zinc and iron degradation

The IBS scaffolds after extracting with acetonitrile were then ultrasonically cleaned for 30 min to collect the residual zinc in NaOH solution (1 mol/L) with full immersion, which was then adjusted to a certain volume for zinc concentration testing with atomic absorption spectroscopy (AAS, 240FS AA, Agilent Technologies, USA). The weight loss of zinc element for each scaffold could be calculated from the original zinc weight and the residual zinc element weight at follow-ups.

After extracting with acetonitrile and cleaning in NaOH solution, the IBS scaffolds were then ultrasonically cleaned in tartaric acid (3–5 wt%), NaOH solution (1 mol/L), deionised water, and absolute ethyl alcohol in sequence to eliminate the iron degradation products. The dried scaffolds were weighed by balance (MSE6.6S, Sartorius, Germany) for calculation of iron weight loss, which has been verified to be an effective method [43].

2.6. Semi-quantitative evaluation of in vivo iron degradation with OCT

Seven typical abdominal aorta segments implanted with 7 IBS scaffolds in 6 New Zealand rabbits and two typical porcine coronary artery segments implanted with 2 IBS scaffolds with both OCT follow-up data and in vivo weight loss data were selected for preliminary verification of the semi-quantitative degradation evaluation method with OCT. The in vivo weight losses by weighing were 1.5 wt%, 6.9 wt%, 24 wt%, 38.3 wt%, 40.6 wt%, 65 wt%, 75 wt%, 87.6 wt%, or 96.7 wt%, as controls for the OCT evaluation. The OCT follow-ups were performed with a commercially available OCT system (C7 XR, LightLab Imaging, St. Jude Medical, Westford, Massachusetts). For semi-quantitative analyses of the iron in vivo degradation, the OCT frames were analysed at 0.2 mm intervals in the implanted segment, and iron struts in the crossing-sections were classified and counted.

2.7. Statistical analysis

Data were expressed as means ± standard deviation. Minitab 17 software was used for data analysis and a value of $P \leq 0.05$ was considered statistically significant. We carried out t tests for the endothelialization and in vivo drug-eluting and degradation evaluation. One-way analysis of variance (ANOVA) followed by post hoc Turkey's multiple comparison tests were conducted for the semi-quantitative degradation evaluation with OCT.

3. Results

3.1. Device design of IBS

The IBS consists of scaffold platform and coating, as illustrated in Fig. 1. The scaffold has a backbone made of an iron tube incorporated with about 0.05 wt% nitrogen, with two sets of gold radiopaque markers of plum blossom shape located at both ends to enhance the visibility, and an 800 nm pure zinc buffer layer on the scaffold backbone. The zinc layer is aimed to prevent the IBS iron backbone from degradation within 3 months after implantation. The scaffold surface was coated with asymmetric sirolimus-loaded biodegradable PDLLA layers, so that most of sirolimus were concentrated on the abluminal side of the stent, which is helpful for inhibiting the proliferation of smooth muscle cells. The total strut thickness of the IBS scaffold is only 73 μm and the low profile of the IBS system (around 1.04 mm) makes it possible to be delivered to target lesion in coronary artery through 5 French guiding catheter. It is easier to transport and store IBS since the relevant temperature is no more than 30 °C, while polymeric BRSs need usually to be transported using cold chain and stored in ice box under low temperature (≤10 °C).

Although the Absorb scaffold was withdrawn from market in 2017 after getting CE mark and FDA approval, there are so far still 5 CE marked BRSs on market, including ART (164 μm, 2015), Magmaris (170 μm, 2016), Fantom (125 μm, 2017), DESolve Cx (120 μm, 2017), and MeRes100 (100 μm, 2019) as shown in Fig. S1, indicating a tendency of the decreasing strut thickness of BRS. Two thick-strut BRSs which approved recently by China National Medical Products Administration (NMPA) are Neovas (170 μm, 2019) and Xinsorb (160 μm, 2020). Except for the magnesium-based Magmaris scaffold, all the above BRSs on market are polymeric. IBS is the only iron-based bioresorbable scaffold in the world having come into clinical studies (First-In-Man clinical trial in 2018) [19], which is as thin as the permanent ultra-thin strut stent Orsiro and much thinner than the state-of-the-art permanent thin strut stent Xience.

3.2. Endothelial coverage and endothelial function restoration

We examined the in vivo efficacy of the IBS in a rabbit model using Xience stents as control. Fig. 2A shows typical cobblestone-shaped morphologies of endothelial cells on the inner surfaces of IBS Z8-P20 and Xience after 45 days of implantation in rabbit iliac arteries. As shown in Fig. 2B, endothelial coverage on struts of IBS Z8-P20 (100.0% ± 0.0%) is significantly greater than that of Xience (81.9% ± 18.1%) at day 45 after implantation ($P = 0.034$), indicating a better endothelialization of the IBS. The endothelial coverage between struts of IBS Z8-P20 (99.7% ± 0.4%) is also significantly greater than that of Xience (90.8% ± 8.3%) at day 45 after implantation ($P = 0.026$). While the rabbit individual variance of endothelialization both on and between struts of Xience by SEM was significant, there was no significant individual variance of endothelialization of IBS Z8-P20.

The confocal images in Fig. 3A further demonstrate typical cobblestone-shaped morphologies of endothelial cells on the inner surfaces of IBS Z8-P20 and Xience after 45 days of implantation in rabbit iliac arteries. Regions 1 and 3 represent areas with a competent endothelial barrier recognized by strong co-localization of p120/VE-cadherin showing light yellow endothelial borders, which is a mixture of red and green channel; regions 2 and 4 showing green borders mostly indicate areas with VE-cadherin poorly expressed at endothelial cell borders leading to poor barrier function. Endothelialization evaluated by functional endothelial coverage is defined as the percentage of the area with a competent endothelial barrier recognized by strong co-localization of VE-cadherin/p120 showing endothelial borders of light yellow, which is a mixture of red and green channel in confocal microscopy. There is no statistical significance ($P = 0.673$) of endothelialization evaluated by functional endothelial coverage on struts of IBS Z8-P20 (59.2% ± 31.5%) and Xience (51.8% ± 27.6%). There is also no statistical significance ($P = 0.706$) of endothelialization evaluated by functional endothelial coverage between struts of IBS Z8-P20 (55.9% ± 33.5%) and Xience (49.1% ± 27.3%).

3.3. In vivo degradation profiles in two animal models and influence of design parameters

We also examined in vivo degradation and drug-eluting profiles in rabbit and porcine models. As shown in Fig. 4, except for the result at day 28 (0.0 wt% ± 0.0 wt% vs 0.0 wt% ± 0.0 wt%), the iron degradation of IBS Z8-P20 in the rabbit model was much faster ($P < 0.05$) than in the porcine model (15.6 wt% ± 10.2 wt% vs 0.0 wt% ± 0.0 wt% at day 90; 24.1 wt% ± 9.8 wt% vs 0.3 wt% ± 0.6 wt% at day 180). Zinc degradation of IBS Z8-P20 in the rabbit model are 28.5 wt% ± 11.0 wt% after 28 days of implantation, 69.1 wt% ± 10.7 wt% after 90 days implantation and 77.8 wt% ± 8.8 wt% after 180 days of implantation.

It could also be seen from Fig. S2 that the sirolimus release rates of IBS Z8-P20 in the rabbit abdominal aorta model are much higher ($P < 0.05$) than those in the porcine coronary artery model at day 60,
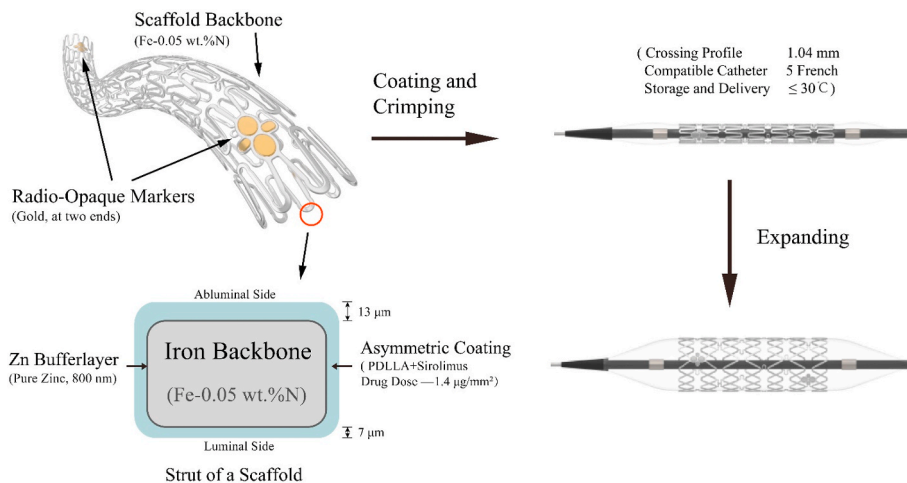
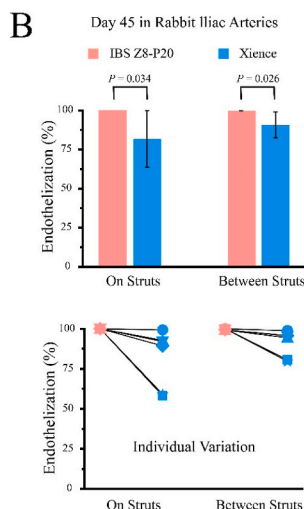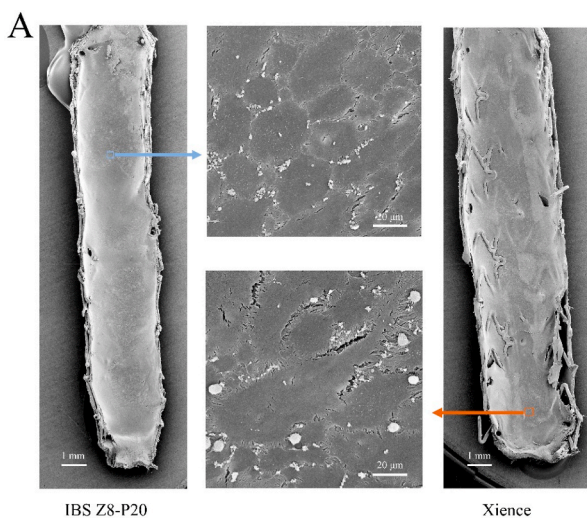**Fig. 1.** Schematic presentation of design of the sirolimus-eluting iron bioresorbable scaffold (IBS).

Fig. 2. (A) SEM images to show representative morphologies of endothelial cells on the inner surfaces of IBS and Xience; (B) endothelialization extents evaluated by endothelial coverage both on struts and between struts directly compared in each individual animal between IBS Z8-P20 and Xience after 45 days of implantation in rabbit iliac arteries observed in a scanning electron microscope. The line between the pink and blue dots indicate that these two dots come from the same rabbit, but in two different iliac arteries. For each group, $n = 6$.

90 and 180 after implantation, while there are no statistical differences within 28 days after implantation.

The design parameters of three IBSs which differ in the thickness of zinc buffer layer and PDLLA coating are shown in Fig. 5A. Fig. 5B shows a significant difference of zinc degradation rates between IBS Z8-P20 and IBS Z8-P13 within 90 days after implantation (28.5 wt% $\pm$ 11.0 wt% vs 14.5 wt% $\pm$ 8.1 wt% at day 28, $P = 0.002$; 71.4 wt% $\pm$ 10.0 wt% vs 56.7 wt% $\pm$ 18.3 wt% at day 90, $P = 0.03$), while there is no statistical difference ($P > 0.05$) of zinc degradation rates after 180 days of implantation in rabbit abdominal aorta (79.3 wt
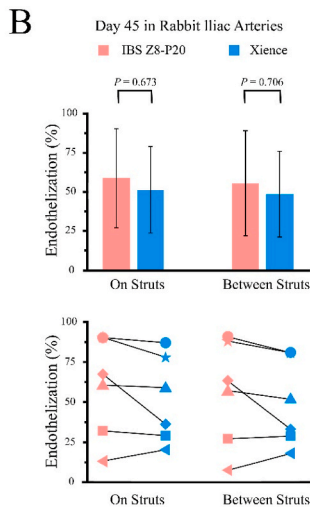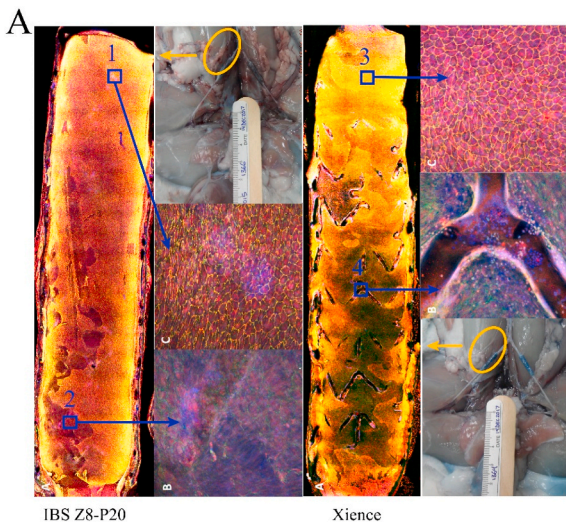

Fig. 3. (A) Representative confocal morphological images of dual immunofluorescent staining of VE-Cadherin and P120 for functional endothelial coverage on the luminal surfaces of IBS Z8-P20 and Xience; (B) endothelialization extents evaluated by functional endothelial coverage both on struts and between struts using confocal microscopy compared between IBS Z8-P20 and Xience in each individual rabbit after 45 days of implantation in iliac arteries. The line between the pink and blue dots indicate that these two dots come from the same rabbit, but in two different iliac arteries. For each group, $n = 6$. Note: VE-cadherin is represented by the red channel (555 nm), with p120 green channel (488 nm), while the blue channel (405 nm) is for the DAPI counterstain. Functional endothelial coverage is defined as the percentage of the area with a competent endothelial barrier recognized by strong co-localization of VE-cadherin/p120 showing endothelial borders of light yellow, which is a mixture of red and green channel.
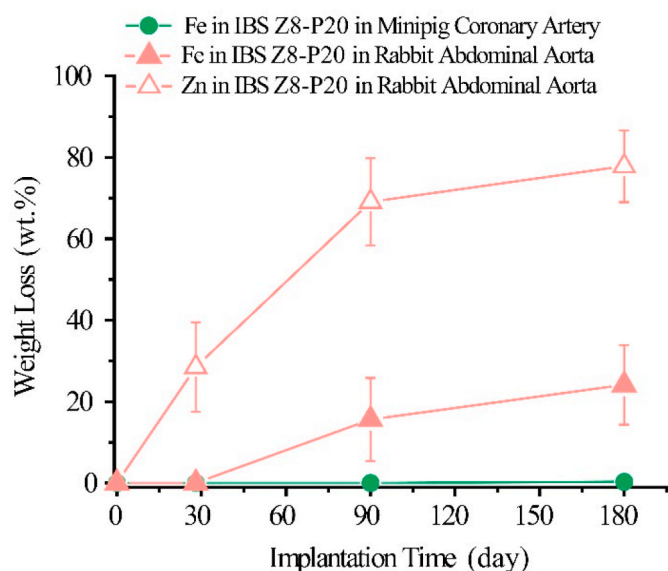
Fig. 4. Zinc weight loss of IBS Z8-P20 in rabbit abdominal aorta, iron weight loss of IBS Z8-P20 in minipig coronary artery and rabbit abdominal aorta.

% ± 7.5 wt% vs 76.7 wt% ± 6.8 wt%). IBS Z8-P20 and IBS Z8-P13 kept iron scaffolds intact at day 28 after implantation and then exhibited significant difference of iron degradation after 90 days of implantation (14.9 wt% ± 9.0 wt% vs 2.7 wt% ± 2.5 wt%, $P = 0.000$); no significant difference of iron degradation could be found after 180 days of implantation (31.8 wt% ± 14.0 wt% vs 18.9 wt% ± 12.6 wt %, $P = 0.092$). The drug-eluting profiles are similar for IBS Z8-P20 scaffold, IBS Z8-P13 scaffold and 316L SS P13 stent without any significant difference ($P > 0.05$), as shown in Fig. S3.

The influence of thickness of the zinc buffer layer is shown in Fig. 5C. A significant difference of iron degradation rate could be found between IBS Z6-P13 scaffold and IBS Z8-P13 scaffold in a hybrid implantation mode after 3 months of implantation in rabbit abdominal

artery (19.4 wt% ± 14.2 wt% vs 2.6 wt% ± 5.1 wt% at day 90, $P = 0.004$). The iron degradation of IBS Z6-P13 in the nine different rabbits range from 2.5 wt% to 42.4 wt% indicating huge individual variation, while that of IBS Z8-P13 are mostly around 0.3 wt% with only one singular result of 16.2 wt%.

3.4. Semi-quantitative method for degradation evaluation with OCT

We suggested a semi-quantitative method to evaluate in vivo iron degradation using OCT. The basic principle is presented in Fig. 6 with the help of some typical experiment images. The original iron strut immediately after implantation was defined as case 0, in which the radial height (thickness) is T_0. Case 0 is accompanied with a sharply delineated bright structure with shadowing behind completely shielding deeper vessel structures within the vessel wall in a cross-sectional OCT frame. Before significant degradation, the iron strut embedded in neointima is slightly deformed or dimmed (case 1), with radial height around T_0. As illustrated in case 0 in Fig. 6, in case that the struts connect with each other to form a continuous bright structure much longer than the normal length, the long bright structure should be counted as two or more struts of case 0 or 1 to avoid underestimate of the struts of no or low degradation.

Since the iron degradation products diffuse to the surrounding in the duration of degradation, the outline of the luminal surface of the iron strut delineated by iron degradation products would change into arched highlight area with shadowing behind (bow area) in OCT. Consequently, the radial height (T) of the bow area formed after iron degradation could be used to identify the iron degradation degree (d). Each case of a degraded strut indicates a specific value of T, which corresponds to a certain iron degradation degree. For semi-quantitative calculation, radial height of $2T_0$ in case 2 strut means 20% iron degradation (d_2), radial height of $3T_0$ in case 3 strut means 50% iron degradation (d_3) and radial height of no less than $4T_0$ in case j strut means almost full degradation of the iron scaffold (d_j). For an over 50% degraded iron scaffold, quite a few struts have been bioresorbed and indiscernible in OCT, N_{j+1} and d_{j+1} (100%) could be introduced to modify the evaluation result. Other cases should belong to one of these
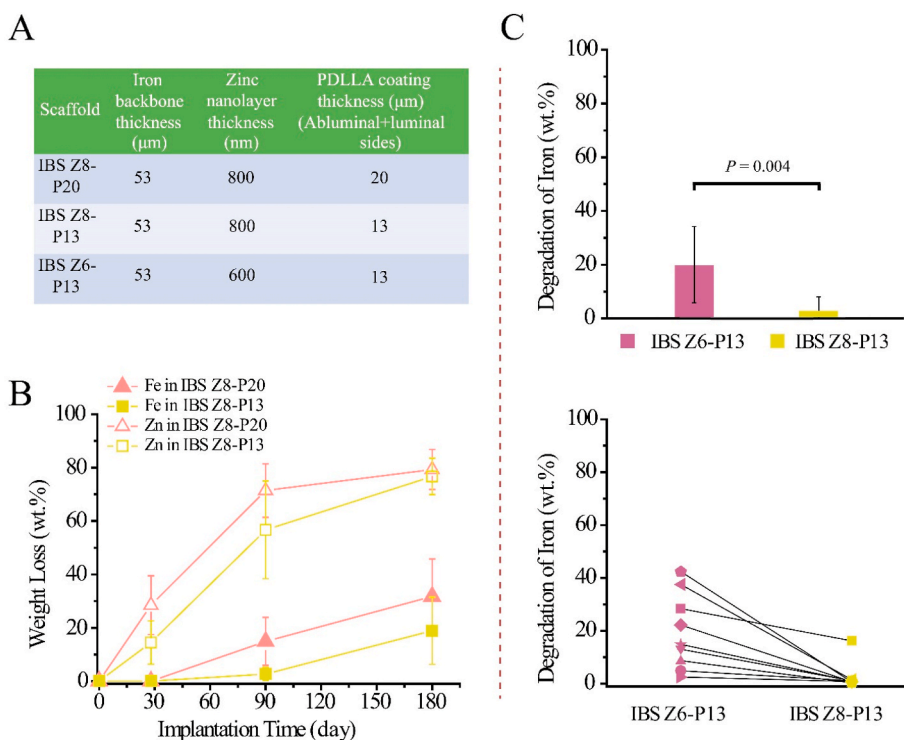
Fig. 5. (A) The design parameters of three IBSs; (B) iron and zinc weight losses of IBS Z8-P20 and IBS Z8-P13 scaffolds in rabbit abdominal aorta; (C) comparison of iron degradation rate and the effect of rabbit individual variance on iron degradation between IBS Z6-P13 scaffold and IBS Z8-P13 scaffold after 3 months of implantation in rabbit abdominal artery. The line between the purple dots and yellow dots indicate that these two dots come from the same rabbit abdominal artery.

Scaffold	Iron backbone thickness (μm)	Zinc nanolayer thickness (nm)	PDLLA coating thickness (μm) (Abluminal+luminal sides)
IBS Z8-P20	53	800	20
IBS Z8-P13	53	800	13
IBS Z6-P13	53	600	13

Fig. 6. Illustration of a semi-quantitative method to evaluate in vivo iron degradation using optical coherence tomography (OCT). The "Initial" refers to the stage after implantation immediately. Case 0 is the typical example of the initial stage where the radial height (thickness) is T_0 and the strut is sharply delineated bright structure with shadowing behind completely shielding deeper vessel structures. Case 1 is an example of nearly 0% degradation which is characterized by the iron strut slightly deformed or dimmed, with the radial height still around T_0. In case that two or more struts connect with each other to form a bright structure much longer than the normal length, the long bright structure should be counted as two or more struts of type 0 or 1 to avoid underestimate of the struts of no or low degradation. After degradation, the degradation products will diffuse to the surrounding, making a nearly arched highlight area with shadowing in OCT as shown in case 2, case 3 and case j. The radial height (T) of the bow area could be used to identify the iron degradation degree (d). For example, radial height of $2T_0$ in case 2 strut means probably 20% iron degradation (d_2), radial height of $3T_0$ in case 3 strut means probably 50% iron degradation (d_3) and radial height of no less than $4T_0$ in type j strut refers to almost full degradation of the iron scaffold (d_j). In any samples, iron degradation could be semi-quantitatively calculated by accumulating $N_n \times d_n$. For iron scaffold of more than 50% degradation, since some struts have been bioresorbed and indiscernible in OCT, N_{j+1} and d_{j+1} (100%) should be introduced to modify the evaluation result.

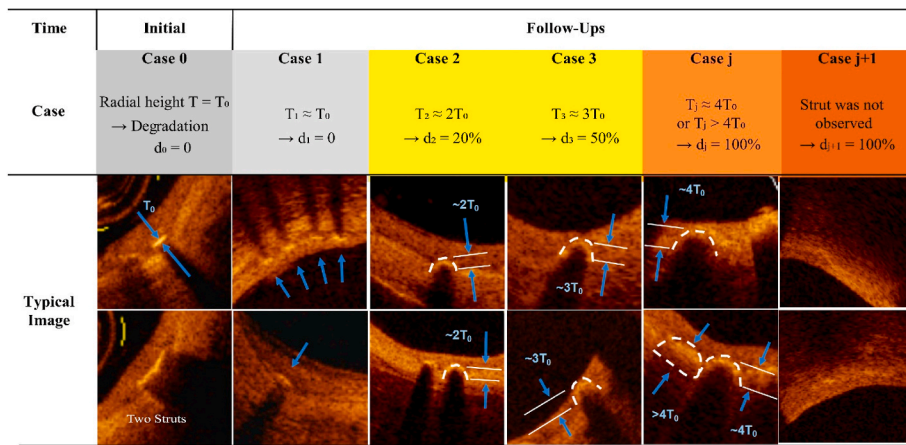five cases based on the radial height. For example, if the radial height is closer to $2T_0$ than to $3T_0$, the iron degradation degree should be set as 20% rather than 50%. It is worth noting that a linear interpolation could be done between these pairs of T_j-d_j in order to be closer to the real degradation.

At any follow-up time, iron degradation could be semi-quantitatively calculated by accumulating $N_n d_n$ (n from 1 to j or j + 1) using the identified radial height T of the bow area, the corresponding degradation degree d and the total strut number N of the same case in all cross-sectional OCT frames, as shown in Fig. S4. The total number of struts N_j is equal to the accumulation of N_{jn} (n from 1 to i), namely accumulation of the number of struts of the same case in all cross-sectional OCT frames at 0.2 mm longitudinal intervals within the stented vessel segment along the automatically constructed lumen centre-line.

Fig. 7A presents an example of using the semi-quantitative method to evaluate iron degradation of an 8 mm long iron-based scaffold. All struts in each of the 2-dimensional (cross-sectional) OCT frames from 3-dimensional OCT video were first evaluated for iron degradation and were then presented in an unfolded scaffold state with identified spatial locations and degradation rates (0% degradation in grey rectangle, partially degradation in light yellow rectangle, and 100% degradation in brown rectangle). The iron degradation results by the semi-quantitative method are compared to those by the widely-used weighing

method with nine samples of representative weight losses ranging from 1.5 wt.% to 96.7 wt%. As shown in Fig. 7B, the weight loss of iron by OCT is close to that by weighing, showing a high accuracy of this semi-quantitative method.

If we denote weight loss calibrated via OCT as WL(OCT) and that via weighing as WL(weigh), the maximum absolute error of |WL(OCT) – WL(weigh)| is no more than 7.4 wt%, and the maximum relative error (RE) is no more than 20.8% except for samples 1 and 2 with very low iron degradation, as shown in Table 1. So, the measurements using the semi-quantitative OCT method had high coincidence with those by the weighing method. The iron degradation of the nine samples could be distinguished from each other by the OCT semi-quantitative method since there were statistically significant differences between measurements of any two of the nine samples.

We further evaluated the repeatability of this novel semi-quantitative method by three tests for each sample and reproducibility by three testers. Each tester independently conducted three tests for each of the three samples (6.9 wt%, 65.0 wt% and 96.7 wt%) using the semi-quantitative method. The maximum standard deviation of WL(OCT) is no more than 3.1 wt% and the maximum relative standard deviation is no more than 8.4% except for sample 1 and 2 with very low iron degradation. Hence, the repeatability of the semi-quantitative method is acceptable. The data of samples 2, 6 and 9 from duplicate tests are of
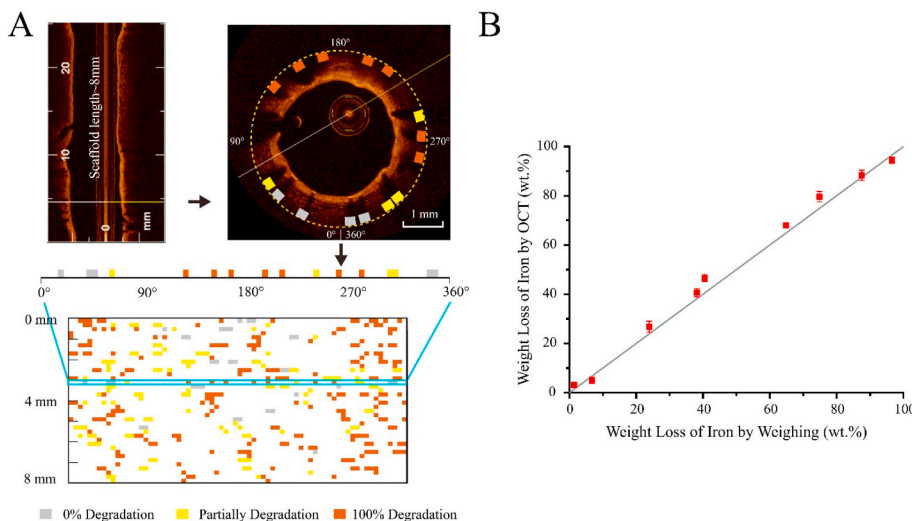
Fig. 7. (A) Example of using the semi-quantitative method to evaluate iron degradation of an 8 mm long iron-based scaffold and present the spatial location of struts with identified different degrees of degradation (0% in grey rectangle, partially degradation in light yellow rectangle, and 100% degradation in brown rectangle) in an unfolded scaffold state, from 3-dimensional OCT video to 2-dimensional (cross-sectional) OCT frames and then to each strut cross-section. (B) Comparison of the results by the semi-quantitative OCT method to those by the widely-used weighing method with nine samples of representative weight losses ranging from 1.5 wt% to 96.7 wt%.

Table 1
Comparison of the results by the semi-quantitative OCT method to those by the widely-used reliable weighing method with nine samples of representative weight losses.

Degradation of Iron		Sample 1	Sample 2	Sample 3	Sample 4	Sample 5	Sample 6	Sample 7	Sample 8	Sample 9
Scaffold product design		IBS Z8-P20	IBS Z8-P13	IBS Z8-P20	IBS Z8-P20	IBS Z8-P20	IBS Z8-P20	IBS Z8-P20	IBS Z8-P20	IBS Z8-P20
Animal Models		Porcine coronary artery	Rabbit abdominal aorta	Rabbit abdominal aorta	Porcine coronary artery	Rabbit abdominal aorta	Rabbit abdominal aorta	Rabbit abdominal aorta	Rabbit abdominal aorta	Rabbit abdominal aorta
Follow-up Time (Month)		6	3	6	12	9	18	18	36	36
WL(weigh) (wt.%)		1.5	6.9	24.0	38.3	40.6	65.0	75.0	87.6	96.7
WL(OCT) (wt.%) Mean ± SD (n)	Tester 1	3.2 ± 0.4 (3)	5.1 ± 1.3 (3)	26.8 ± 2.3 (3)	40.7 ± 1.7 (3)	46.7 ± 1.5 (3)	68.0 ± 1.0 (3)	79.7 ± 2.1 (3)	88.3 ± 2.1 (3)	94.5 ± 1.3 (3)
	Tester 2	/	5.8 ± 2.0 (3)	/	/	/	68.9 ± 1.1 (3)	/	/	96.6 ± 1.0 (3)
	Tester 3	/	9.2 ± 1.0 (3)	/	/	/	62.7 ± 3.1 (3)	/	/	92.6 ± 1.1 (3)
RSD of WL(OCT)	Tester 1	10.9%	24.7%	8.4%	4.3%	3.3%	1.5%	2.6%	2.4%	1.4%
	Tester 2	/	33.5%	/	/	/	1.6%	/	/	1.0%
	Tester 3	/	11.4%	/	/	/	4.9%	/	/	1.2%
Error$_{min}$ ~ Error$_{max}$ of |WL(OCT) – WL (weigh)| (wt.%)		1.4–2.1	0.4–3.1	0.5–5.0	0.6–3.8	4.4–7.4	1.0–5.0	3.0–7.0	1.4–2.4	0.2–5.1
RE$_{min}$ ~ RE$_{max}$ of |WL(OCT) – WL (weigh)| (%)		93.3–113.3	5.8–44.9	2.1–20.8	1.7–10.8	10.8–18.2	1.5–7.7	4.0–9.3	1.6–2.7	0.2–5.3

low variation with maximum standard deviation no more than 3.4 wt%, which demonstrates the good reproducibility of the semi-quantitative method.

4. Discussion

4.1. Advantages of design of the novel iron bioresorbable scaffold

The prerequisite of a BRS is noninferiority to the state-of-the-art permanent drug-eluting stent, and then the bioresorbable performance could be considered as an additional valuable benefit. As demonstrated in the real world clinical practices, a thin strut has not only become the development trend of the current generation permanent drug-eluting stents but also the future direction of BRS [21,22,44]. Consensus from an expert panel about the optimal BRS considerations include: 1) thinner struts; 2) lower profile; 3) adequate radial force; 4) no or low thrombogenic risks; 5) complete absorption within 6–12 months [1,21]. All of the above depend on appropriate materials. Withdrawn of Absorb scaffolds made of PLA [45] might be due to the insufficient mechanical performance of the polyester, which leads to thick strut design and big crossing-profile to ensure sufficient radial strength, and therefore the PLA scaffold is difficult to deliver and has slower endothelial coverage and higher thrombosis risk. Additionally; microstructural heterogeneity within the PLA scaffold leads to asymmetric degradation, which might cause scaffold discontinuities, malapposition and consequent thrombosis [34]; the scaffold material PLA is processed to provide sufficient supporting within 6 months after implantation, however the complete degradation from 2 to 4 years depends on the crystallization of PLLA [46] and the period with undesirable risks is also prolonged.

By virtue of the excellent mechanical performance of iron-based alloy [47], IBS is one of the thinnest BRSs in the world (Fig. S1). It has comparable low crossing-profile, 5 French guiding catheter compatibility, mechanical strength, specification range, endothelialization, safety and effectiveness to state-of-the-art permanent drug-eluting stents [36,48] in vitro and in animal models. As presented in Fig. 2, IBS has significantly faster endothelial coverage than the Co–Cr alloy stent Xience, which illustrates the advantage of IBS than Xience. Compared with thicker strut stents, the thinner strut of the iron based stent owing to the excellent mechanical property of this metal brings with convenience of operation in interventional treatment and is beneficial for rapid endothelial coverage that are related with decreased stent thrombosis. A previous study by Virmani et al. showed that the drug in a stent coating to resist proliferation of smooth muscle cells in media might cause inhibition of the endothelial function restoration [42]. As shown in Fig. 3, the comparable endothelial function restoration of IBS to Xience after 45 days of implantation in rabbit iliac arteries suggests that the comprehensive effect of zinc and PDLLA degradation products and drug release of IBS is similar to the effect of released drug of Xience. The inherent drawback of slow degradation of iron in near neutral local tissue environment had been overcome by tuning of a PDLLA coating with a complete degradation period around or within 1.5 years [36]. And our previous study has demonstrated the IBS scaffold is MR (magnetic resonance) conditional, similar to permanent metallic drug-eluting stents [49]. Besides, IBS could be delivered and stored at a temperature of no more than 30 °C while the majority of polymer-based BRSs should be transported and stored below 10 °C. Although safety and effectiveness still need to be demonstrated in clinical trials, the novel iron-based scaffold has the potential to avoid drawbacks and risks of PLA scaffolds to become a potentially ideal BRS.

4.2. Species differences, individual variation and their effects on BRS design

According to Fig. 5B and Fig. S3, the PDLLA amount, the only difference between IBS Z8-P20 and IBS Z8-P13 scaffolds, causes significantly different degradation rates of zinc and iron after 90 days of implantation in the same animal model while the drug release rate

maintains similar. Further, although IBS Z8-P13 releases zinc and iron degradation products while 316L SS P13 does not, both of them have a similar drug release profile owing to the same drug-eluting coating in the same animal model. Nevertheless, even the same IBS scaffold has significantly different degradation rates of iron and release rates of drug in different animal models, which implies that the degradation rates of the drug-loaded coating is influenced by local environment of implantation position. To sum up, the degradation rates of zinc and iron and drug release rates of IBS are influenced by the degradation of PDLLA coating and the microenvironment of an implant. Endothelialization of permanent metallic stents in porcine coronary artery was ever reported to be much faster than that in rabbit iliac artery, and the latter is faster than that in human diseased coronary artery [24]. Consequently, for properties like degradation and endothelialization which are greatly influenced by local environment of implantation, there might be significant differences between different implantation positions and animal species, namely different animal models.

According to Fig. 4, the degradation of iron of IBS in rabbit abdominal aorta is much faster than that in porcine coronary artery. Although abundant animal studies had been conducted for Absorb PLLA BRS and Magmaris magnesium BRS in pre-clinical stage, both Absorb and Magmaris had been iterated to decrease degradation after the first-in-human clinical study. It might be inferred that the degradation of polymer-based bioresorbable scaffold and magnesium-based bioresorbable scaffold in human diseased coronary artery might all be faster than that in rabbit abdominal aorta and porcine coronary artery. Our iron-based bioresorbable scaffold might be in a similar situation.

Normally, an animal model cannot accurately predict all the risks after implantation in human, and it is suggested to choose different animal models having the closest performance to that in human or challenging the worst case of environment regarding every specific in vivo property for effective evaluation so as to guide product design iteration before initiating a clinical study. For example, US Food and Drug Administration recommends rabbit iliac artery rather than minipig coronary artery as a model to evaluate endothelialization for permanent drug-eluting coronary stents. Besides, minipig healthy coronary artery is acknowledged to be the suitable animal model for safety (fracture, embolism, thrombosis, local tissue responses etc.) and effectiveness (stenosis) evaluation, and pharmacokinetics study of coronary stents. Rodent (mouse or rat) is the preferred animal species to evaluate systemic toxicity. Since permanent vascular stents with durable coating do not degrade after implantation, the effect of local environment of different animal species on stent performance and effectiveness is small. In contrast, for a sirolimus-eluting iron bioresorbable scaffold, the present study has demonstrated that the degradations of the PDLLA coating and iron matrix are slower in porcine healthy coronary artery, leading to slower drug release. It is recommended that the rabbit iliac arteries injured by balloon endothelial denudation are used for endothelialization, degradation, drug release and stenosis evaluation of IBS. On the other hand, a porcine coronary model can mimic the fatigue loading of human coronary artery, over-dilation and release of degradation products, and it is particularly susceptible to severe local tissue responses after implantation of a bioresorbable scaffold.

Figs. 2B, 3B and 5C also illustrate animal individual variation of properties like endothelialization and degradation, which are greatly influenced by local environment of implantation. While individual variation means the requirement of a large number of samples, one prefers, from the ethical perspective, as much reliable data for novel medical implants with as few animals as possible. To minimize the impact of individual variation on evaluation of important in vivo performance, reasonable experiment design and sample size selection are crucial. Implanting both the experimental group and the control group of stents in a hybrid mode in two separate but the same type of vessels is recommended, such as left and right coronary arteries in a porcine model, left and right iliac arteries in a rabbit model, as well as left and right anterior tibial artery in a canine model. Besides, based on the

results of this study, we recommend that no less than 3 animals with 6 or more samples should be used for a pre-experiment and no less than 5 animals with 10 or more samples should be used for a formal experiment. If data from a pre-study show great variation, a larger number of samples should be examined in the formal study.

For the IBS scaffold, the pure zinc buffer layer is employed to delay the onset of the degradation of iron scaffold backbone. By increasing thickness of the zinc buffer layer, the iron scaffold backbone could stay intact without degradation for a longer time after implantation. As demonstrated in Fig. 5C, an 800 nm zinc buffer layer in IBS Z8-P13 could protect iron scaffold backbone from degradation for three months after implantation in rabbit abdominal, while the 600 nm zinc buffer layer in IBS Z6-P13 scaffold could not resist the rabbit individual variation with the fluctuated iron degradation rates. Considering the manufacturing tolerance and animal individual variation, a product should have adequate design safety margin to the lower control limit concerning some properties susceptible to service-environment, to ensure meeting the technical requirements under all possible conditions.

4.3. Possible factors to influence in vivo performance of bioresorbable scaffolds

We would like to categorize the factors that influence in vivo performance of implants and cause animal model difference and individual variation as follow: A) physical factors, B) chemical factors and C) biological responses, as schematically illustrated in Fig. S5. The effect of local environment on bioresorbable implants is stronger than that on the permanent implants, since the microenvironment is much dynamic along with the biodegradation.

For the physical factors, the shear stress from blood flow influences endothelialization, and the blood temperature influences degradation of polymers (e.g. PDLLA). Different implantation positions have different biomechanical loads, such as vasomotion under cyclic high and low blood pressures, radial compression from expanded lesion vessel, plaques, tension and bending in coronary arteries with heartbeats, tension in pulmonary blood vessels with breathing, direct compression of vessel wall, tension, bending and torsion with limb movement or external force in below-the-knee vessels. Further, the biomechanical loads might cause stress corrosion or corrosion fatigue of a bioresorbable stent, which accelerate degradation as usual.

For the chemical factors, different pH values of body fluids in different animal models or animal individuals might have significant effects on degradation of bioresorbable metals and polymers. Enzymes can also accelerate polymer degradation, which may further accelerate zinc and iron degradation and drug release. Oxygen content in blood and tissue fluids determines the phases of iron degradation products: an oxygen-poor environment is favourable for the formation of magnetic magnetite, which are compact deposits in the tissue and difficult to be engulfed by the macrophages; an oxygen-rich environment is favourable for the formation of nonmagnetic ferric oxide or iron oxyhydroxide particles, which are dispersed in the tissue and easy to be engulfed by the macrophages for bioresorption. Fast bioresorption of the iron degradation products allows the residual iron to continue to degrade without a blocking effect, consequently showing faster degradation. High contents of ions of Ca^{2+}, PO_4^{3-}, etc. in the blood or tissue fluids, severe calcification, or high contents of lipid composition in the plaques might cause complete coverage of a Ca–P layer, a hydrated iron phosphate layer or a lipid layer on the scaffolds to prevent penetration of water and oxygen, which thereby decrease iron degradation [50]. Ions of Cl^- and SO_4^{2-} are likely to cause pit corrosion, leading to the local acceleration of iron degradation [51]. What's more, Cl^- is also notorious for zinc degradation [52], which may have influence on the degradation of iron. In addition, endothelial cell coverages on struts of permanent stents and bioresorbable scaffolds are normally lower than those between struts, which is strengthened in Fig. 2B for a permanent Xience stent after 45 days of implantation in rabbit iliac arteries. In

contrast, the endothelial cell coverage on struts of every IBS Z8-P20 scaffold in Fig. 2B is, despite no statistical significance, higher than that between struts of the same scaffold on average, which implies that the ions of iron and/or zinc from degradation might be a bit beneficial for coverage of endothelial cells.

Biological responses are stimulated after the implantation of a foreign body [53], which might also influence the in vivo performance of an implant. For example, if inflammation caused by the foreign body implantation in the lesion vessel lowers the pH value of the local tissue, the degradation of PLA, zinc and iron in IBS embedded in the local tissue would be accelerated. A bioresorbable stent in the fibrin or endothelial cell layer after endothelialization might exhibit different degradation rates from the bioresorbable scaffold exposed in the blood flow flush. When embedded in the neointima, the acidic degradation products of PDLLA might be easy to accumulate to form local environment of low pH to further accelerate the PDLLA coating degradation, zinc and iron corrosion, and drug release of IBS. In contrast, when exposed in the blood flow, the degradation of the PDLLA coating and iron might be slower in the neutral environment due to blood buffer capacity. Fibrosis and calcification might decrease the iron degradation by alleviating water and oxygen penetration. Besides, transferrin and macrophages could clear free iron ions released to blood and solid degradation products of PDLLA and iron depositing in tissue, which might in turn enhance the dissolution of iron [51]. Different animal models or animal individuals exhibit varied response extents and varied numbers of transferrins and macrophages, which might partially account for the dependence of biodegradation rates of IBS on animal types and individuals. The drug release changes also with the degradation rate in different animal models or animal individuals, and further influences the effectiveness and safety of a bioresorbable scaffold.

In different animal models (animal species and specific implantation positions), further experiments are needed to identify the controlling factors of each specific property, so as to better predict the performance in human using the animal experiment data.

4.4. Semi-quantitative approach to measure iron degradation in a non-destructive way & verification of repeatability and reproducibility of the new method

Weight loss is a reliable and classic way to evaluate the degradation of biomaterials in animal experiments. Nevertheless, this method is not suitable for human clinical follow-up at all, since it needs to explant the implanted device. In our previous work and other researches, IVUS and OCT have been demonstrated to be capable of evaluating iron, magnesium or polymer degradation qualitatively [20,36,54–57]. Using OCT to evaluate the degradation of polymer-based bioresorbable scaffold qualitatively had also been proved feasible for human clinical follow-up [58]. The present study has further established a set of criteria to evaluate the iron degradation semi-quantitatively with OCT.

We compared the OCT semi-quantitative method to the weight loss method. As shown in Fig. 7 and Table 1, the tested values using the OCT method were close to those using the weight loss method with the maximum absolute error less than 7.4% for all samples and the relative error less than 10% for samples of iron degradation more than 65 wt%. This illustrates the accuracy of our measurement with the OCT method. The precision of the tested results of different times and different testers using the OCT method were also examined; the repeatability and reproducibility were confirmed to be acceptable for a semi-quantitative method with the standard deviation less than 5 wt% for all samples and the relative standard deviation less than 10% for samples of iron degradation more than 24 wt%.

4.5. Study limitations

The present work examined in vivo degradation performance of an ultrathin iron bioresorbable scaffold in limited animal models. The data were pooled from multiple studies instead of directly obtained from an independently designed study. Manufacturing tolerance and abnormalities shall also contribute to the individual variation of in vivo performance to some extent.

5. Conclusions

We designed and fabricated a biodegradable stent IBS using the technique of metal-polymer composite. The endothelial coverage on the luminal surface of IBS was significantly faster than that of the commercialized nonbiodegradable Xience stent while the function restoration of the endothelial cells on the IBS was comparable to that on the Xience after 45 days of implantation in the rabbit iliac arteries. The ultrathin strut in IBS might be beneficial to the excellent endothelial cell coverage, while many factors including degradation products and released drug could influence the endothelial function restoration. The present work demonstrated significant species differences of stent or scaffold degradation between minipig and rabbit, and significant animal individual variation of endothelialization and degradation. Therefore, there should be adequate design window in conducting product iteration in animal models to enable the iron bioresorbable scaffold applicable in human body. Hybrid implantation modes and sufficient animal numbers have been suggested to use for obtaining reliable animal experiment data. In order to guide product design iteration before clinical studies, it is also advised to choose suitable animal models with the closest performance to that in human when comparing different properties.

In the present study, a semi-quantitative method with OCT has been established and verified to evaluate biodegradation of iron. Compared with the conventional weight loss method, this novel methodology affords a non-destructive way to monitor the in vivo biodegradation of IBS scaffold, which is of much importance for the later clinical trial and follow-ups of a bioresorbable coronary stent.

Associated content

Supporting Information associated with this article can be found, in the online version, at doi: ***. Summary of the strut thicknesses of different bioresorbable scaffolds (BRSs); drug-eluting profiles of a sirolimus-eluting iron bioresorbable scaffold (IBS), IBS Z8-P20 in minipig coronary artery and rabbit abdominal aorta; drug-eluting profiles of IBS Z8-P20 scaffold, IBS Z8-P13 scaffold, and 316L stainless steel P13 stent in rabbit abdominal aorta; illustration of a semi-quantitative evaluation method of in vivo iron degradation using OCT; possible factors influencing in vivo performance of implants and causing animal model difference and individual variation.

Declaration of competing interest

It is declared that Wenjiao Lin, Wanqian Zhang, Haiping Qi, Li Qin, Haifeng Li, Xiaoli Shi and Deyuan Zhang are employees of Biotyx Medical (Shenzhen) Co., Ltd, and Gui Zhang is an employee of Shenzhen Advanced Medical Services Co., Ltd. The other authors declare no conflict of interest.

Acknowledgements

Appendix A. Supplementary data

Supplementary data to this article can be found online at https://doi.org/10.1016/j.bioactmat.2020.09.020.

CRediT authorship contribution statement

W.Z., D.Z., R.G. and J.D. conceived the concept. W.L., W.Z., D.Z., R.G. and J.D. designed the experiments. J.D., D.Z., W.L., and H.Z. carried out most of data analysis and manuscript writing. All of the authors joined in pertinent experiments and manuscript writing.

References

[1] S. Bangalore, H.G. Bezerra, D.G. Rizik, E.J. Armstrong, B. Samuels, S.S. Naidu, The state of the absorb bioresorbable scaffold-consensus from an expert panel, JACC Cardiovasc. Interv. 10 (2017) 2349–2359.

[2] S.G. Ellis, D.J. Kereiakes, D.C. Metzger, R.P. Caputo, D.G. Rizik, P.S. Teirstein, M.R. Litt, A. Kini, A. Kabour, S.O. Marx, J.J. Popma, R. McGreevy, Z. Zhang, C. Simonton, G.W. Stone, Everolimus-eluting bioresorbable scaffolds for coronary artery disease, N. Engl. J. Med. 373 (20) (2015) 1905–1915.

[3] D.J. Kereiakes, Y. Onuma, P.W. Serruys, G.W. Stone, Bioresorbable vascular scaffolds for coronary revascularization, Circulation 134 (2) (2016) 168–182.

[4] R. Rehman, M.C. Marhisham, M. Alwi, Stenting the complex patent ductus arteriosus in tetralogy of Fallot with pulmonary atresia: challenges and outcomes, Future Cardiol. 14 (2018) 55–73.

[5] H. Sallmon, F. Berger, M.Y. Cho, B. Opgen-Rhein, First use and limitations of Magmaris(R) bioresorbable stenting in a low birth weight infant with native aortic coarctation, Cathet. Cardiovasc. Interv. 93 (7) (2019) 1340–1343.

[6] R.L. Varcoe, O. Schouten, S.D. Thomas, A.F. Lennox, Experience with the absorb everolimus-eluting bioresorbable vascular scaffold in arteries below the knee: 12-month clinical and imaging outcomes, JACC Cardiovasc. Interv. 9 (16) (2016) 1721–1728.

[7] S. Nishio, K. Kosuga, K. Igaki, M. Okada, E. Kyo, T. Tsuji, E. Takeuchi, Y. Inuzuka, S. Takeda, T. Hata, Y. Takeuchi, Y. Kawada, T. Harita, J. Seki, S. Akamatsu, S. Hasegawa, N. Bruining, S. Brugaletta, S. de Winter, T. Muramatsu, Y. Onuma, P.W. Serruys, S. Ikeguchi, Long-term (> 10 years) clinical outcomes of first-in-human biodegradable poly-l-lactic acid coronary stents: Igaki-Tamai stents, Circulation 125 (19) (2012) 2343–2353.

[8] J. Bennett, Q. De Hemptinne, K. McCutcheon, Magmaris resorbable magnesium scaffold for the treatment of coronary heart disease: overview of its safety and efficacy, Expet Rev. Med. Dev. 16 (9) (2019) 757–769.

[9] K. Xu, G.S. Fu, B. Xu, Y.J. Zhou, X. Su, H.L. Liu, Z. Zhang, B. Yu, X.Z. Wang, Y.L. Han, Safety and efficacy of the novel sirolimus-eluting bioresorbable scaffold for the treatment of de novo coronary artery disease: one-year results from a prospective patient-level pooled analysis of NeoVas trials, Cathet. Cardiovasc. Interv. 93 (S1) (2019) 832–838.

[10] Y.Z. Wu, L. Shen, J.S. Yin, J.H. Chen, J.Y. Qian, L. Ge, J.B. Ge, Twelve-month angiographic and clinical outcomes of the XINSORB bioresorbable sirolimus-eluting scaffold and a metallic stent in patients with coronary artery disease, Int. J. Cardiol. 293 (2019) 61–66.

[11] B.J. Forrestal, B.C. Case, C. Yerasi, H.M. Garcia-Garcia, R. Waksman, The Orsiro ultrathin, bioresorbable-polymer sirolimus-eluting stent: a review of current evidence, Cardiovasc. Revascularization Med. 21 (2020) 540–548.

[12] J.F. Iglesias, O. Muller, D. Heg, M. Roffi, D.J. Kurz, I. Moarof, D. Weilenmann, C. Kaiser, M. Tapponnier, S. Stortecky, S. Losdat, E. Eeckhout, M. Valgimigli, A. Odutayo, M. Zwahlen, P. Jüni, S. Windecker, T. Pilgrim, Biodegradable polymer sirolimus-eluting stents versus durable polymer everolimus-eluting stents in patients with ST-segment elevation myocardial infarction (BIOSTEMI): a single-blind, prospective, randomised superiority trial, Lancet 394 (10205) (2019) 1243–1253.

[13] D.E. Kandzari, J.J. Koolen, G. Doros, J.J. Massaro, H.M. Garcia-Garcia, J. Bennett, A. Roguin, E.G. Gharib, D.E. Cutlip, R. Waksman, B.V. Investigators, Ultrathin bioresorbable polymer sirolimus-eluting stents versus thin durable polymer everolimus-eluting stents, J. Am. Coll. Cardiol. 72 (25) (2018) 3287–3297.

[14] D.E. Kandzari, J.J. Koolen, G. Doros, H.M. Garcia-Garcia, J. Bennett, A. Roguin, E.G. Gharib, D.E. Cutlip, R. Waksman, Ultrathin bioresorbable-polymer sirolimus-eluting stents versus thin durable-polymer everolimus-eluting stents for coronary revascularization: 3-year outcomes from the randomized BIOFLOW V trial, JACC Cardiovasc. Interv. 13 (11) (2020) 1343–1353.

[15] D. Regazzoli, P.P. Leone, A. Colombo, A. Latib, New generation bioresorbable scaffold technologies: an update on novel devices and clinical results, J. Thorac. Dis. 9 (Suppl 9) (2017) S979–S985.

[16] M. Iantorno, M.J. Lipinski, H.M. Garcia-Garcia, B.J. Forrestal, T. Rogers, D. Gajanana, K.D. Buchanan, R. Torguson, W.S. Weintraub, R. Waksman, Meta-analysis of the impact of strut thickness on outcomes in patients with drug-eluting stents in a coronary artery, Am. J. Cardiol. 122 (10) (2018) 1652–1660.

[17] H. Jinnouchi, S. Torii, A. Sakamoto, F.D. Kolodgie, R. Virmani, A.V. Finn, Fully bioresorbable vascular scaffolds: lessons learned and future directions, Nat. Rev. Cardiol. 16 (5) (2019) 286–304.

[18] A. Seth, Y. Onuma, R. Costa, P. Chandra, V.K. Bahl, C. Manjunath, A. Mahajan, V. Kumar, P. Goel, G. Wander, M. Kalarickal, U. Kaul, V.K.A. Kumar, P. Rath, V. Trehan, G. Sengottuvelu, S. Mishra, A. Abizaid, P.W. Serruys, First-in-human evaluation of a novel poly-L-lactide based sirolimus-eluting bioresorbable vascular scaffold for the treatment of de novo native coronary artery lesions: MeRes-1 trial, EuroIntervention 13 (4) (2017) 415–423.

[19] B. Xu, K. Dou, R. Gao, Iron-based BRS: Design Features, Experimental Studies, and FIM Experience, (2018) TCT2018.

[20] L. Song, Z.W. Sun, C.D. Guan, H.B. Yan, M.Y. Yu, J.A. Cui, C.W. Mu, H. Qiu, Y.D. Tang, Y.Y. Zhao, S.B. Qiao, H. Suryapranata, R.L. Gao, B. Xu, First-in-man study of a thinner-strut sirolimus-eluting bioresorbable scaffold (FUTURE-I): three-year clinical and imaging outcomes, Cathet. Cardiovasc. Interv. 95 (Suppl 1) (2020) 648–657.

[21] A. Sakamoto, H. Jinnouchi, S. Torii, R. Virmani, A.V. Finn, Understanding the impact of stent and scaffold material and strut design on coronary artery thrombosis from the basic and clinical points of view, Bioengineering (Basel) 5 (3) (2018).

[22] N. Foin, R.D. Lee, R. Torii, J.L. Guitierrez-Chico, A. Mattesini, S. Nijjer, S. Sen, R. Petraco, J.E. Davies, C. Di Mario, M. Joner, R. Virmani, P. Wong, Impact of stent strut design in metallic stents and biodegradable scaffolds, Int. J. Cardiol. 177 (3) (2014) 800–808.

[23] S.H. Im, Y. Jung, S.H. Kim, Current status and future direction of biodegradable metallic and polymeric vascular scaffolds for next-generation stents, Acta Biomater. 60 (2017) 3–22.

[24] A.V. Finn, G. Nakazawa, M. Joner, F.D. Kolodgie, E.K. Mont, H.K. Gold, R. Virmani, Vascular responses to drug eluting stents: importance of delayed healing, Arterioscler. Thromb. Vasc. Biol. 27 (7) (2007) 1500–1510.

[25] S. Nakatani, Y. Ishibashi, Y. Sotomi, L. Perkins, J. Eggermont, M.J. Grundeken, J. Dijkstra, R. Rapoza, R. Virmani, P.W. Serruys, Y. Onuma, Bioresorption and vessel wall integration of a fully bioresorbable polymeric everolimus-eluting scaffold: optical coherence tomography, intravascular ultrasound, and histological study in a porcine model with 4-year follow-up, JACC Cardiovasc. Interv. 9 (8) (2016) 838–851.

[26] A. Hideo-Kajita, S. Wopperer, V.B. Seleme, M.H. Ribeiro, C.M. Campos, The development of magnesium-based resorbable and iron-based biocorrodible metal scaffold technology and biomedical applications in coronary artery disease patients, Appl. Sci. 9 (17) (2019).

[27] H. Cubero-Gallego, B. Vandeloo, J. Gomez-Lara, R. Romaguera, G. Roura, J.A. Gomez-Hospital, A. Cequier, Early collapse of a magnesium bioresorbable scaffold, JACC Cardiovasc. Interv. 10 (18) (2017) e171–e172.

[28] J. Bayon, M. Santas-Alvarez, R. Ocaranza-Sanchez, C. Gonzalez-Juanatey, Magmaris very late in-scaffold restenosis: has the "black boxes" nightmare come back? Cathet. Cardiovasc. Interv. (2019) 1–3.

[29] L.B. Wu, J.D. Ding, In vitro degradation of three-dimensional porous poly(D,L-lactide-co-glycolide) scaffolds for tissue engineering, Biomaterials 25 (27) (2004) 5821–5830.

[30] Y.M. Peng, Q.J. Liu, T.L. He, K. Ye, X. Yao, J.D. Ding, Degradation rate affords a dynamic cue to regulate stem cells beyond varied matrix stiffness, Biomaterials 178 (2018) 467–480.

[31] J.D. Ding, A composite strategy to fabricate high-performance biodegradable stents for tissue regeneration, Science China Materials 61 (8) (2018) 1132–1134.

[32] D. Bian, J.X. Deng, N. Li, X. Chu, Y. Liu, W.T. Li, H. Cai, P. Xiu, Y. Zhang, Z.P. Guan, Y.F. Zheng, Y.H. Kou, B.G. Jiang, R.S. Chen, In vitro and in vivo studies on biomedical magnesium low-alloying with elements gadolinium and zinc for orthopedic implant applications, ACS Appl. Mater. Interfaces 10 (5) (2018) 4394–4408.

[33] J. Gonzalez, R.Q. Hou, E.P.S. Nidadavolu, R. Willumeit-Romer, F. Feyerabend, Magnesium degradation under physiological conditions - best practice, Bioact Mater 3 (2) (2018) 174–185.

[34] P.J. Wang, N. Ferralis, C. Conway, J.C. Grossman, E.R. Edelman, Strain-induced accelerated asymmetric spatial degradation of polymeric vascular scaffolds, Proc. Natl. Acad. Sci. U. S. A. 115 (11) (2018) 2640–2645.

[35] N. Artzi, N. Oliva, C. Puron, S. Shitreet, S. Artzi, A. bon Ramos, A. Groothuis, G. Sahagian, E.R. Edelman, In vivo and in vitro tracking of erosion in biodegradable materials using non-invasive fluorescence imaging, Nat. Mater. 10 (9) (2011) 704–709.

[36] W.J. Lin, D.Y. Zhang, G. Zhang, H.T. Sun, H.P. Qi, L.P. Chen, Z.Q. Liu, R.L. Gao, W. Zheng, Design and characterization of a novel biocorrodible iron-based drug-eluting coronary scaffold, Mater. Des. 91 (2016) 72–79.

[37] Y.L. Qi, H.P. Qi, Y. He, W.J. Lin, P.Z. Li, L. Qin, Y.W. Hu, L.P. Chen, Q.S. Liu, H.T. Sun, Q. Liu, G. Zhang, S.Q. Cui, J. Hu, L. Yu, D.Y. Zhang, J.D. Ding, Strategy of metal-polymer composite stent to accelerate biodegradation of iron-based biomaterials, ACS Appl. Mater. Interfaces 10 (1) (2018) 182–192.

[38] Y.L. Qi, X. Li, Y. He, D.Y. Zhang, J.D. Ding, Mechanism of acceleration of iron corrosion by a polylactide coating, ACS Appl. Mater. Interfaces 11 (1) (2019) 202–218.

[39] X. Li, W.Q. Zhang, W.J. Lin, H. Qiu, Y.L. Qi, X. Ma, H.P. Qi, Y. He, H.J. Zhang, J. Qian, G. Zhang, R.L. Gao, D.Y. Zhang, J.D. Ding, Long-term efficacy of biodegradable metal-polymer composite stents after the first and the second implantations into porcine coronary arteries, ACS Appl. Mater. Interfaces 12 (13) (2020) 15703–15715.

[40] L.W. Jiao, G. Zhang, P. Cao, D.Y. Zhang, Y.F. Zheng, R.X. Wu, L. Qin, G.Q. Wang, T.Y. Wen, Cytotoxicity and its test methodology for a bioabsorbable nitrided iron stent, J. Biomed. Mater. Res. B Appl. Biomater. 103 (4) (2015) 764–776.

[41] B. Liu, Y.F. Zheng, Effects of alloying elements (Mn, Co, Al, W, Sn, B, C and S) on biodegradability and in vitro biocompatibility of pure iron, Acta Biomater. 7 (3) (2011) 1407–1420.

[42] H. Mori, Q. Cheng, C. Lutter, S. Smith, M. Guo, M. Kutyna, S. Torii, E. Harari, E. Acampado, M. Joner, F.D. Kolodgie, R. Virmani, A.V. Finn, Endothelial barrier protein expression in biodegradable polymer sirolimus-eluting versus durable

polymer everolimus-eluting metallic stents, JACC Cardiovasc. Interv. 10 (23) (2017) 2375–2387.

[43] W.J. Lin, L. Qin, H.P. Qi, D.Y. Zhang, G. Zhang, R.L. Gao, H. Qiu, Y. Xia, P. Cao, X. Wang, W. Zheng, Long-term in vivo corrosion behavior, biocompatibility and bioresorption mechanism of a bioresorbable nitrided iron scaffold, Acta Biomater. 54 (2017) 454–468.

[44] C. Costopoulos, T. Naganuma, A. Latib, A. Colombo, Looking into the future with bioresorbable vascular scaffolds, Expert Rev. Cardiovasc Ther. 11 (10) (2013) 1407–1416.

[45] A. Colombo, L. Azzalini, Bioresorbable scaffolds-a complex journey to the promised land, JACC Cardiovasc. Interv. 10 (2017) 2360–2362.

[46] J. Iqbal, Y. Onuma, J. Ormiston, A. Abizaid, R. Waksman, P. Serruys, Bioresorbable scaffolds: rationale, current status, challenges, and future, Eur. Heart J. 35 (2014) 765–776.

[47] Y.Y. Li, J.L. Yan, W.H. Zhou, P. Xiong, P. Wang, W. Yuan, Y.F. Zheng, Y. Cheng, In vitro degradation and biocompatibility evaluation of typical biodegradable metals (Mg/Zn/Fe) for the application of tracheobronchial stenosis, Bioact Mater 4 (2019) 114–119.

[48] J.F. Zheng, H. Qiu, Y. Tian, X.Y. Hu, T. Luo, C. Wu, Y. Tian, Y. Tang, L.F. Song, L. Li, L. Xu, B. Xu, R.L. Gao, Preclinical evaluation of a novel sirolimus-eluting iron bioresorbable coronary scaffold in porcine coronary artery at 6 months, JACC Cardiovasc. Interv. 12 (3) (2019) 245–255.

[49] D. Bian, L. Qin, W.J. Lin, D.N. Shen, H.P. Qi, X.L. Shi, G. Zhang, H.W. Liu, H. Yang, J. Wang, D.Y. Zhang, Y.F. Zheng, Magnetic resonance (MR) safety and compatibility of a novel iron bioresorbable scaffold, Bioact. Mater. 5 (2) (2020) 260–274.

[50] R. Tolouei, J. Harrison, C. Paternoster, S. Turgeon, P. Chevallier, D. Mantovani, The use of multiple pseudo-physiological solutions to simulate the degradation behavior of pure iron as a metallic resorbable implant: a surface-characterization study, Phys. Chem. Chem. Phys. 18 (29) (2016) 19637–19646.

[51] Y.F. Zheng, X.N. Gu, F. Witte, Biodegradable metals, Mater. Sci. Eng. R Rep. 77 (2014) 1–34.

[52] Y. Meng, L. Liu, D. Zhang, C. Dong, Y. Yan, A.A. Volinsky, L.N. Wang, Initial formation of corrosion products on pure zinc in saline solution, Bioact. Mater. 4 (1) (2019) 87–96.

[53] S.D. Rousselle, Y. Ramot, A. Nyska, N.D. Jackson, Pathology of bioabsorbable implants in preclinical studies, Toxicol. Pathol. 47 (3) (2019) 358–378.

[54] H.M. Garcia-Garcia, P.W. Serruys, C.M. Campos, T. Muramatsu, S. Nakatani, Y.J. Zhang, Y. Onuma, G.W. Stone, Assessing bioresorbable coronary devices: methods and parameters, JACC Cardiovasc. Imaging 7 (11) (2014) 1130–1148.

[55] Y. Onuma, P.W. Serruys, L.E. Perkins, T. Okamura, N. Gonzalo, H.M. Garcia-Garcia, E. Regar, M. Kamberi, J.C. Powers, R. Rapoza, H. van Beusekom, W. van der Giessen, R. Virmani, Intracoronary optical coherence tomography and histology at 1 month and 2, 3, and 4 years after implantation of everolimus-eluting bioresorbable vascular scaffolds in a porcine coronary artery model: an attempt to decipher the human optical coherence tomography images in the ABSORB trial, Circulation 122 (22) (2010) 2288–2300.

[56] T.L.P. Slottow, R. Pakala, T. Okabe, D. Hellinga, R.J. Lovec, F.O. Tio, A.B. Bui, R. Waksman, Optical coherence tomography and intravascular ultrasound imaging of bioabsorbable magnesium stent degradation in porcine coronary arteries, Cardiovasc. Revascularization Med. 9 (4) (2008) 248–254.

[57] R. Waksman, F. Prati, N. Bruining, M. Haude, D. Bose, H. Kitabata, P. Erne, S. Verheye, H. Degen, P. Vermeersch, L. Di Vito, J. Koolen, R. Erbel, Serial observation of drug-eluting absorbable metal scaffold: multi-imaging modality assessment, Circ. Cardiovasc. Interv. 6 (6) (2013) 644–653.

[58] P.W. Serruys, J.A. Ormiston, Y. Onuma, E. Regar, N. Gonzalo, H.M. Garcia-Garcia, A bioabsorbable everolimus-eluting coronary stent system (ABSORB): 2-year outcomes and results from multiple imaging methods, Lancet 373 (2009) 897–910.